RSC Advances

ROYAL SOCIETY OF CHEMISTRY

www.rsc.org/advances

Influence of CrB_2 target current on the microstructure, mechanical and tribological properties of Cr-B-C-N coatings in water

Qiang Ma [a,b], Fei Zhou [a,b*], Qianzhi Wang [a,b], Zhiwei Wu [a,b], Kangmin Chen [c], Zhifeng Zhou [d], Lawrence Kwok-Yan Li [d]

[a] *State Key Laboratory of Mechanics and Control of Mechanical Structures, Nanjing University of Aeronautics and Astronautics, Nanjing, 210016, China*

[b] *College of Mechanical and Electrical Engineering, Nanjing University of Aeronautics and Astronautics and Jiangsu Key Laboratory of Precision and Micro-Manufacturing Technology, Nanjing, 210016, China*

[c] *Center of Analysis, Jiangsu University, Zhenjiang, 212013, China*

[d] *Department of Mechanical and Biomedical Engineering, City University of Hong Kong, Hong Kong, China*

Abstract: Cr-B-C-N coatings with different boron contents (24.6-27.2 at.%) were deposited on Si(100) wafers and 316L stainless steels by using closed-field unbalanced magnetron sputtering via adjusting the CrB_2 target current. The microstructures, mechanical and tribological properties of Cr-B-C-N coatings in water were characterized by using XRD, XPS, SEM, nano-indentation and ball-on-disk tribometers. The results showed that the soft amorphous BN phases were formed when boron elements were introduced into CrCN coatings. With an increase in the CrB_2 target current, the B content increased from 24.9 to 27.2 at.%, which caused the a-BN content in CrBCN coatings increasing gradually, and then the hardness of CrBCN coatings decreased from 18.6±0.86 GPa to 16.3±0.28 GPa. Due to the formation of H_3BO_3, the friction coefficient and wear rates of CrBCN/SiC tribopairs were lower than those of CrCN/SiC tribopairs. When the CrBCN coatings (25.1 at.% B) were deposited at the CrB_2 target current of 3 A, the lowest values of friction coefficient (0.16) and wear rate (2.1×10^{-7} mm^3/Nm) were obtained simultaneously.

Keywords: Cr-B-C-N coatings; Microstructure; Mechanical properties; Friction and wear; Water lubrication

[*]Corresponding author. Tel./Fax: +86 25 84893083.

E-mail address: fzhou@nuaa.edu.cn(F. Zhou)

1. Introduction

In comparison to the conventional oil lubrication system, water lubrication system is an effective way to save energy sources and to protect natural environment. However, water possesses a relatively low viscosity and a strong corrosion ability, which restrains its wide application for metallic materials. A promising approach to solve this technical problem is to modify the surface properties of metallic materials by depositing hard coatings with a good lubricity in water. Currently, the carbon-based and transition metal nitride-based coatings have been deemed to be the promising surface coatings on the sliding parts in water hydraulic system [1, 2]. Although the carbon-based coatings, such as diamond, DLC, a-CN_x and GLC, exhibited low friction coefficients and wear rates in water, their practical applications have been limited owing to the poor adhesion to the substrates originating from their high internal stress [3-6]. But for the transition metal nitride-based coatings such as TiN-based coatings, due to the high hardness, strong wear resistance, good chemical inertness, thermal stability and great adhesion to the substrate, they have been widely utilized as protective hard coatings [7, 8]. As compared with the TiN coatings, TiCN coatings as a combination of TiN and TiC showed superior wear resistance due to their high hardness and the formation of self-lubricate carbon, while the TiBN coatings consisting of TiN, TiB_2, c-BN and a-BN phases exhibited the advantageous properties for cutting applications due to high hardness, strong toughness and great thermodynamic stability at high temperatures [9-14]. To meet the demand for the advanced coatings, quaternary TiBCN coatings have attracted researchers' concerns due to the super hardness, good tribological properties and strong corrosion resistance and oxidation resistance [15-17]. In comparison to the TiN-based coatings, the CrN-based coatings exhibited a superior corrosion and oxidation resistance and a lower internal stress [18-20]. As seen in Table 1 in Ref. [21], it is clear that the

friction coefficients of the CrN-based coatings sliding against different balls in water environment varied in the range of 0.079-0.56, while the specific wear rates of the CrN-based coatings changed from the magnitude of 10^{-9} to 10^{-5} mm^3/Nm. This indicates that the CrN-based coatings could be used in water environment. However, pure CrN coatings could not be qualified under some extreme conditions because of a relatively low hardness in comparison to pure TiN coatings. Thus, carbon or boron element has been proposed being added into CrN coatings to improve their mechanical properties, so as to enhance the corresponding tribological properties in water [22-24]. It has been demonstrated that the hardness and wear resistance of CrN coatings were enhanced after carbon incorporation [25, 26]. Wang et al. [26] have reported that the hardness of CrCN coatings with 15.35 at.% C reached 22.5 GPa, higher than that (18.5 GPa) of CrN coatings. Moreover, when CrCN coatings slid against Si_3N_4 ceramic balls in water, a low friction coefficient (0.197) was obtained due to the formation of amorphous carbon or carbon nitride layer acting as a solid lubricant at contact area. On the other hand, when boron element was added into the CrN coatings, the CrBN coatings presented a nanocomposite structure consisting of CrN crystallite and amorphous BN phase [27, 28]. Due to a smaller grain size and the interaction between crystallite phase and amorphous phase, CrBN coatings exhibited higher hardness than CrN coatings. Zhang et al. [28] reported that the CrBN coatings with 6.1 at.% B exhibited a maximum hardness (~24 GPa) and a minimum wear rate (0.04 μm^3/Nm) in comparison with the other coatings. Furthermore, the self-lubricating $B(OH)_3$ films resulted from a spontaneous chemical reaction between water molecules and B_2O_3 could contribute to a low friction coefficient when the boride coatings were under friction tests in high humidity environment [29]. Thus, quaternary CrBCN coatings are expected to present better tribological performance in water than CrCN and CrBN coatings. However, up to now, the friction and wear behaviors of CrBCN

coatings in water environment have not yet been studied.

In here, Cr-B-C-N coatings with various boron contents were deposited on Si wafers and 316L stainless steels using unbalanced magnetron sputtering system by way of adjusting the CrB_2 target current. The microstructures, mechanical and water-lubricated tribological properties of Cr-B-C-N coatings were investigated, and then the influences of boron content on the microstructure, mechanical and tribological properties were systematically discussed.

2. Experimental details

2.1 Deposition of Cr-B-C-N coatings

Cr-B-C-N coatings were deposited on Si(100) wafers and 316L stainless steel disks using closed-field unbalanced magnetron sputtering system (UDP-650, Teer Coatings Limited, UK), where two pure chromium targets (99.95%), one pure carbon target (99.95%) and one CrB_2 target (99.9%) were mounted. The coatings deposited on Si(100) wafers were used for the characterizations of EDS, XRD, XPS and SEM, while those on 316L disks were used for the friction tests in tap water. At first, 316L stainless steel disks with dimensions of Φ30 mm×4 mm were polished to a surface roughness (Ra) of 30 nm by using a metallographic polishing machine (UNIPOL-820). Then the as-received Si (100) wafers and the polished 316L disks were ultrasonically cleaned in ethanol and deionized water for 20 minutes before being fixed on substrate holder. Then the background pressure of deposition chamber was pumped down to about 4×10^{-4} Pa and the substrate holder was kept rotating continuously around its central axis at a speed of 10 rpm. Prior deposition, Ar sputtering plasma generated at a bias voltage of -450 V was conducted for 30 minutes to further clean the residual contaminations and oxide layers on the substrate surface, and then a Cr adhesive layer (~0.2 μm) was deposited in advance to enhance the adhesive strength between the substrate and coating. All the coatings were deposited by sputtering

in a mixture of Ar and N_2 gases without shielding to restrict the interaction of gas and plasma streams. The inert Ar gas was used as working gas (0.17 Pa), while N_2 was introduced as the reactive gas (~0.06 Pa) to form nitride coatings. During the sputtering process, the N^+ ion energy was mainly determined by the bias voltage, and the closed filed configuration contributed to the increase of ion density in the plasma. If the bias voltage was too high, coating delamination would be induced due to higher inert stress. If the bias voltage was less than -40 V, the microstructure of coatings would become softer and porous because of the insufficient ion bombardment. Thus, the bias voltage was set as -80 V, and the flow rate of argon was fixed at 50 sccm, while the nitrogen flow rate was controlled by optical emission monitor (OEM) of a constant value of 50% controlled through a piezo-value driven by a computer. Because the substrates were biased, which could attract the ions and then the resulting ion bombardment during coating deposition could cause the temperature rise of the substrates, and there was no extra heater to heat the substrates. A floating thermocouple was placed near the rotating substrate holder. The substrate temperature was approximately 150□ due to ion bombardment. The chamber pressure applied on the holder was maintained at 0.23 Pa. The sputtering current of Cr and C targets was set as 4 A for each target, while the CrB_2 target current varied in the range of 0-4 A to adjust the addition amount of B in the coatings. If the CrB_2 target current was higher than 4 A, the CrB_2 target began to crack due to overheating caused by higher sputtering power. According to CrB_2 target current, the Cr-B-C-N coatings in the next section were denoted as CrCN, CrBCN-1, CrBCN-2, CrBCN-3 and CrBCN-4, respectively. The total depositing time was about one and a half hours, and the detailed parameters of Cr-B-C-N coatings were listed in Table 1.

2.2 Characterization of Cr-B-C-N coatings

The morphology of Cr-B-C-N coatings was examined using a field emission scanning electron

microscope (FESEM) (JEOL-JSM-7001F) equipped with an additional EDS (Inca Energy 350, Oxford, UK). The crystallite phase of Cr-B-C-N coatings was identified by X-ray diffraction (XRD, Ultima IV, Japan) with a Cu Kα (λ=0.15404 nm) radiation source from 20° to 80° at a scanning speed of 5°/min. The bonding structures of coatings were characterized by X-ray photoelectron spectroscopy (ESCALAB 250, Thermo Scientic, UK) using a Al Kα (1486.6 eV) source at 184 W (10.8 mA and 15.2 kV), and the spot size was about 0.5 mm in diameter, meanwhile, the spectrometer resolution was less than 0.62eV. The XPS analysis was performed in the depth of 3-10nm from surface of coatings under a base pressure of 3×10^{-8} Pa by using the Thermo Avantage software. Before measurement, the sample surface was sputtered and etched by Ar ion bombardment for 30 s for surface cleaning. The C_{1s} binding energy line at 284.6 eV was taken as a reference for calibration and the composition was calculated from the peaks areas taking into account the sensitivity factors. In order to get the detailed volume fraction of bonds, Cr 2p, B 1s, C 1s and N 1s fractal spectra were deconvoluted using XPS 4.1 software based on a Lorentzian (20%) and Gaussian (80%) function with nonlinear Shirley-type background.

The hardness and reduced elastic modulus of coatings were measured using a nanoindentor equipped with a Berkovich tip (ENT-1100a, Elionix Co.Ltd., Japan) based on Oliver and Pharr method. Each sample has been measured for 36 times with a penetration depth of 100 nm to ensure the reliability of data and minimize the substrate effect. To assure the reliability of measured data, the corresponding systematic errors were also calculated.

$$\sigma = \sqrt{\frac{\sum_{i=1}^{n} (X_i - \overline{X})^2}{n-1}} \quad (1)$$

where σ, X_i, $\overline{X}$ and n are the standard deviation, the *i*th data point, the average value of all the X_i, and the number of data points, respectively. Then, the final results (as shown in Table 3) could

be quoted according to the following equation:

$$\overline{X} \pm \frac{\sigma}{\sqrt{n}} t_{\alpha/2} \quad (2)$$

where α is the confidence level, here α=1 - 0.95, and $t_{\alpha/2}$ could be found in the relative reference book [30].

The friction tests of Cr-B-C-N coatings sliding against SiC balls in tap water were conducted using a ball-on-disk tribometer at room temperature. The diameter of SiC ball was 8 mm, and its surface roughness, hardness and elastic modulus were 88.5 nm, 22 GPa and 430 GPa, respectively. During the friction tests, the experiments of Cr-B-C-N/SiC tribopairs at the normal load of 3 N and 6 N were conducted, and the sliding velocity and total sliding length were set at 0.1 m/s, and 500 m, respectively. The friction tests were carried out three times to ensure the reliability of data, and to get the mean value of friction coefficient and wear rate. Then, the wear scars of SiC balls and the wear tracks of coatings were observed using an optical microscope (XJZ-6, China), while the cross-section area (A) of wear tracks on the coatings was measured using a 3D profilometer (NanoMap-1000WLI, USA). The specific wear rates of SiC balls and Cr-B-C-N coatings were calculated according to the following Eqs. (1) and (2) :

$$\omega_{s,b} = \frac{\pi d^4}{64RFL} \quad (3)$$

$$\omega_{s,c} = \frac{2\pi rA}{FL} \quad (4)$$

where R is the radius of SiC ball, d is the diameter of the wear scar on the ball, r is the radius of the wear trace on the coating, F is the normal load and L is the total sliding distance.

3. Results and discussion

3.1 Composition, microstructure and morphology of Cr-B-C-N coatings

According to the SEM observation and the EDS analysis, the thickness and chemical

composition of Cr-B-C-N coatings are listed in Table 2. It is obvious that the thickness of coatings increased gradually from 1.40 μm to 1.61 μm as the CrB_2 target current varied from 0 A to 4 A. This indicated that the deposition rate of coatings increased with an increase in the CrB_2 target current. When the CrB_2 target current increased from 0 A to 1 A, the B concentration increased sharply to 24.6 at.%, while the concentrations of Cr, C and N elements all decreased rapidly. With further increasing the CrB_2 target current from 1 A to 4 A, the B element content increased slightly, while the concentrations of Cr, C and N elements all fluctuated slightly. Fig.1 shows the XRD patterns of Cr-B-C-N coatings deposited at the different CrB_2 target currents. As seen in Fig.1, all of the coatings consisted of three peaks centered at 37.5°, 44.5° and 69°. The diffraction peak at 69° was assigned to the Si(100) substrate, while the diffraction peaks at 37.5° and 44.5° were related to CrN/Cr_2N(111) and Cr(110)/CrN/Cr_2N(200) (JCPDS 11-0065, JCPDS 19-0323), respectively, and the Cr(110) was thought to be originated from Cr interlayer [31]. With increasing CrB_2 target current, the diffraction peak at 37.5° became broad with a decreasing intensity. Furthermore, no diffraction peaks related to borides were detected in the XRD pattern, This indicated that the more incorporation of B element could inhibit the crystalline growth of CrN/Cr_2N(111), and the incorporated B might exist as the form of amorphous phase.

Fig.2 shows XPS spectra of Cr 2p, B 1s, C 1s and N 1s for Cr-B-C-N coatings deposited at different CrB_2 target currents, while Fig.3 shows their corresponding fitted results. As seen in Fig.2a, the Cr 2p spectra was deconvoluted into six peaks, which located at 574.4 eV, 575.3 eV, 576.4 eV, 577.8 eV, 584.6 eV and 586.4 eV, respectively. The peak located at 574.4 eV was assigned to Cr-Cr bonds, while the peaks located at 575.3 eV and 576.4 eV were originated from Cr-N bonds [32-34]. The peaks at 577.8 eV, 684.6 eV and 586.4 eV were attributed to Cr-O bonds, this is because that although the deposition chamber pressure was pumped to as low as 4×10^{-4} Pa

before deposition, there was still residual oxygen in chamber and that would react with composition elements of Cr-B-C-N coatings [26]. As seen in Fig.3a, the volume fractions of Cr-Cr and Cr-O bonds both increased to 20.1% and 46.3%, while the volume fraction of Cr-N bonds decreased to 33.6% when the CrB_2 target current increased to 3 A. But as the CrB_2 target current was 4 A, the volume fraction of Cr-Cr bonds decreased to 17.2%, while the volume fraction of Cr-N bonds increased to 36.4%. This indicated that the critical CrB_2 target current for the transformation of bonding structure was 3 A. As seen in Fig.2b, the B 1s spectra could be deconvoluted into three peaks centered at 189.5 eV, 190.2 eV and 192.3 eV, which were corresponded to B-C, B=N and B-O bonds, respectively [35-38]. When the CrB_2 target current increased from 1 A to 4 A, the volume fraction of B-C bonds decreased from 24.3% to 5.2%, while that of B-N bonds increased from 55.5% to 81.0% (Fig.3b). This pointed out that the incorporated B was prone to react with N than C, and then the amorphous BN was gradually formed in Cr-B-C-N coatings. It is clear in Fig.2c that the deconvoluted C1s spectra consisted of three peaks located at 284.7 eV, 286.1 eV and 288.3 eV. The dominant peak at 284.7 eV was assigned to sp^2C-N/sp^2C-C bonds, while the peak located at 286.1 eV was corresponded to sp^3C-N/sp^3C-C bonds [39-41]. Moreover, the peak at 288.3 eV was contributed to C-O bonds [42]. When CrB_2 target current was beyond 1 A, a new peak appeared at 283.5 eV, which was attributed to C-B bonds [43]. When the CrB_2 target current was 0 A, C atoms were mostly existed as sp^2C-N/sp^2C-C bonds with the corresponding volume fraction of 94.9%, which was expected to present a low friction coefficient. When the CrB_2 target current varied in the range of 1 A to 4 A, the volume fraction of sp^2C-N/sp^2C-C bonds fluctuated around 77%, whilst the volume fractions of sp^3C-N/sp^3C-C and C-B bonds increased to 8.0% and 5.0% (Fig.3c), which were beneficial to increasing the hardness of Cr-B-C-N coatings. As seen in Fig.2d, all N 1s spectra consisted of

three peaks which were located at 396.8 eV, 398.2 eV and 399.3 eV, respectively. The dominant peak located at 396.8 eV was attributed to N-Cr bonds, and the peak located at 399.3 eV was attributed to N-C bonds [44, 45]. According to Refs. [46, 47], the peak at 398.2 eV was assigned to N-C and N-B bonds for CrCN coatings and CrBCN coatings accordingly. Based on the above analysis, it is known that the CrCN coatings mainly consisted of Cr-N and C=C bonds, but when the CrB_2 target current was beyond 1 A, the incorporated boron atoms mainly existed as B-N bonds, then the CrBCN coatings mainly contained Cr-N, B-N, C-N and B-C bonds .

The surface topographies and the corresponding surface roughness of Cr-B-C-N coatings deposited at different CrB_2 target currents are shown in Figs.4. As seen in Fig.4a, the surface of CrCN coatings exhibited a clear cauliflower-like morphology and the nanograins were easily distinguished. It was reported that the grain size growth of nanocomposite nitride coatings could be limited when the carbon, silicon or boron was incorporated [31, 48]. As a result, with an increase in the CrB_2 target current, the coatings surface became more compact resulting from a decreasing grain size of cauliflower-like particle. The corresponding average surface roughness (R_a) of CrCN and CrBCN-1 coatings were around 31 nm, with an increasing in the CrB_2 target current to 4 A, the surface roughness decreased monotonically to 16 nm at 4 A. Fig.5 shows the cross-sectional micrographs of Cr-B-C-N coatings, it is obvious that all coatings consisted of Cr interlayer and Cr-B-C-N top layer, and the CrCN coating exhibited typical columnar structure. When the CrB_2 target current varied in the range of 1 A to 4 A, the typical columnar structure gradually disappeared. It is deduced that the formation of amorphous phase would interrupt the columnar growth and then the coatings structure became dense [31].

3.2 Mechanical properties of Cr-B-C-N coatings

The hardness (H) and reduced elastic modulus (E) of Cr-B-C-N coatings deposited at

different CrB_2 target currents are tabulated in Table 3. As seen in Table 3, the hardness and elastic modulus of CrCN coating were 17.7±1.03 GPa and 258±9.59 GPa, respectively. When the CrB_2 target current varied in the range of 1 A-2 A, the hardness of Cr-B-C-N coatings increased slightly to 17.9±0.79 GPa and 18.6±0.86 GPa, respectively. On the one hand, the increasing grain boundary intensities with finer grain size would increase the resistance of dislocation glide, which made a contribution to the increase in hardness of Cr-B-C-N coatings [45]. On the other hand, solid solution effect also contributed to the increase of hardness [28]. However, the gradual formation of soft amorphous BN in CrBCN coatings deposited at the CrB_2 target current of 3 A and 4 A, led to a decrease in the hardness, and then the hardness of CrBCN-4 coating dropped to 16.3±0.28 GPa eventually. The elastic modulus of CrBCN coatings also increased slightly to 261±10.40 GPa when the current of CrB_2 target increased to 2 A at first, and then decreased to 228±2.53 GPa with further increasing the CrB_2 target current to 4 A. As is known, the plasticity index (H/E) and the plastic deformation resistance (H^3/E^2) provide a close correlation with the wear resistance of coatings [39, 49]. As seen in Table 3, the values of H/E and H^3/E^2 increased monotonously when the current of CrB_2 target increased from 0 A to 3 A, and the maximum values of H/E (0.079) and H^3/E^2 (0.113) were all obtained at the CrB_2 target current of 3 A. When the current of CrB_2 target reached 4 A, the values of H/E and H^3/E^2 both decreased. Thus, the CrBCN-3 coating is expected to present a superior tribological performance in water.

3.3 Tribological properties of Cr-B-C-N coatings sliding against SiC balls in tap water

Fig.6 shows the friction behaviors of Cr-B-C-N coatings sliding against SiC balls at 3 N and 6 N in tap water, and Fig.7 shows the contact pressure of Cr-B-C-N/SiC tribopairs at 3 N and 6 N. As seen in Fig.6a, the initial friction coefficient of the CrCN/SiC tribopairs at 3 N was 0.24, higher than those of all CrBCN/SiC tribopairs. In principle, the initial friction coefficient is

proportional to the original contact surface roughness, and the highest initial friction coefficient of CrCN/SiC tribopairs was well consistent with the coarse columnar structure of CrCN coatings (Fig.4a). In addition, the initial friction coefficient was also closely related to the initial contact pressure. According to Hertzian's ball-on-disk mode, the initial contact pressures for the Cr-B-C-N/SiC tribopairs were calculated. As shown in Fig.7a, the CrCN/SiC tribopair showed the highest initial contact pressure of 0.69 GPa (Fig.7a), which also contributed to the higher initial friction coefficient of CrCN/SiC tribopairs. With increasing the sliding distance, the friction coefficient of the CrCN/SiC tribopairs decreased monotonously to 0.18 within 102 m, and then increased gradually to 0.24. When the B element was incorporated into the CrCN coatings, the variation of friction coefficient for the CrBCN/SiC tribopairs was dependent on the CrB_2 target current. Specifically, the friction coefficient of CrBCN-1/SiC tribopairs increased from 0.17 to 0.2 within the first 32 m, while the friction coefficient of CrBCN-2/SiC tribopairs increased from 0.18 to 0.2 within 101 m. When the CrB_2 target current increased to 3 A, the CrBCN-3/SiC tribopairs exhibited the lowest friction coefficient of 0.15 and the friction coefficient fluctuated around 0.16. When the CrB_2 target current reached 4 A, the friction coefficient of CrBCN-4/SiC tribopairs decreased from 0.2 to 0.18 within the first 9 m, and then increased to 0.23 when the sliding distance increased to 163 m. Finally, the friction coefficient increased slightly to 0.25. After the friction tests, the ultimate contact pressure could be calculated by using the formula P=F/S, where F is the normal load and S is the wear contact area of mating balls. As seen in Fig.7a, the ultimate contact pressure ranged from 0.031GPa to 0.074GPa. In order to know the tribological properties of Cr-B-C-N coatings at higher loads, the friction tests sliding against SiC balls at 6 N were conducted in tap water, and the corresponding friction behavior is showed in Fig.6b. As seen in Fig.6b, the friction behavior of CrCN and CrBCN-1 coatings showed the similar tendency,

increased during the running-in period, and then decreased in the next 40 m and 80 m, respectively. With further sliding to 500 m, the friction coefficient showed an increasing tendency, while CrBCN-2, CrBCN-3 and CrBCN-4 coatings fluctuated slightly around 0.15 during the whole sliding process. As seen in Fig.7b, the initial contact pressures for Cr-B-C-N/SiC tribopairs under 6 N ranged from 0.83 GPa to 0.87 GPa. After the friction tests, the ultimate contact pressures varied from 0.45 GPa to 0.107 GPa.

Fig.8 shows the variation of the friction coefficient and specific wear rates for the Cr-B-C-N/SiC tribopairs at the normal load of 3 N with the CrB_2 target current. As seen in Fig.8a, with an increase in the CrB_2 target current, the mean-steady friction coefficient of Cr-B-C-N/SiC tribopairs first decreased from 0.21 to 0.16 at the CrB_2 target current of 3 A, and then increased to 0.22. This indicated that the B incorporation could improve the lubrication properties of coatings to a certain extent. As is known, the specific wear rate of coatings is closely related to the friction coefficient and hardness of coatings. As seen in Fig.8b, the specific wear rate of CrCN coatings was 5.7×10^{-7} mm^3/Nm, while the specific wear rate of CrBCN-1 coatings was 3.9×10^{-7} mm^3/Nm. With further increasing the CrB_2 target current to 3 A, the specific wear rate of CrBCN coatings first increased to 4.1×10^{-7} mm^3/Nm, and then declined to the lowest value of 2.1×10^{-7} mm^3/Nm. When the CrB_2 target current was 4 A, the specific wear rate of CrBCN-4 coating increased quickly to 6.3×10^{-7} mm^3/Nm. It was obvious that the CrBCN coatings deposited at the CrB_2 target current of 3 A exhibited the best tribological properties in water. Moreover, due to the protection of transferred films from coatings to SiC balls, the specific wear rates of SiC balls were all lower than those of Cr-B-C-N coatings [39]. Fig.9 shows the mean-steady friction coefficient of Cr-B-C-N/SiC tribopairs at the normal load of 6 N. As seen in Fig.9, it is clear that the friction coefficients of Cr-B-C-N/SiC tribopairs at 3N were higher than those at 6N. As compared with the

CrCN and CrBCN-1 coatings deposited at the CrB_2 target current of 0 A and 1 A, the Cr-B-C-N coatings deposited at the CrB_2 target current beyond 1A showed a lower friction coefficient (~0.15), this phenomena indicated that incorporated boron could still play a role in decreasing friction coefficient at the normal load of 6 N.

The cross-sectional profiles and optical images with the wear width of the wear tracks on the Cr-B-C-N coatings at the normal load of 3 N are illustrated in Fig.10 and Fig.11. As seen in Fig.10a and Fig.11a, the depth and width of wear track on the CrCN coatings were higher, and some adhering wear debris could be observed on the wear track, meanwhile, there were some grooves parallel to the sliding direction because of abrasive wear. When the CrB_2 target current increased from 1 A to 3 A, the depth and width of wear track increased firstly and then decreased (Fig.10b-d), and the shallowest and narrowest wear track was observed on the Cr-B-C-N coatings deposited at the CrB_2 target current of 3 A (Fig.10d and 11d). But when the CrB_2 target current was 4 A, the wear track on the CrBCN-4 coatings became deeper and wider. As compared with the CrCN coatings, a significant wear could be observed on the wear track of CrBCN-4 coatings (Fig.10e). It is necessary to indicate that when the CrB_2 target current was beyond 0 A, there were fewer grooves on the wear tracks of coatings, and the wear surface became very smooth, thus, the wear mechanism was mainly tribochemical wear. Fig.12 shows the SEM images of the wear tracks and the corresponding EDS analyses of the Cr-B-C-N coatings at 3 N. As seen in Fig.12, the wear track of the CrCN coatings was wide and only Cr, C and N elements appeared in the EDS analysis, while the wear tracks of the CrBCN-1, CrBCN-3 and CrBCN-4 coatings were shallower, and also only Cr, C and N elements were found in the EDS analyses. Furthermore, a clear partial delamination was observed on the wear track of CrBCN-2 coatings (Fig.12e), which was proved by the Fe peaks in the EDS analysis (Fig.12f). Thus, although the CrBCN-2 coatings

exhibited lower friction coefficient in comparison to the CrBCN-1 coatings, the corresponding specific wear rate was higher.

The optical images with the wear width of the wear tracks on the Cr-B-C-N coatings at the normal load of 6 N are illustrated in Fig.13. As seen in Fig.13a, the widths of wear tracks of CrCN and CrBCN-1 coatings were 354.1 μm, and there were obvious abrasive grooves on the wear track. However, when the CrB_2 target current was in the range of 1-4 A, a serious delamination could be observed on the wear track (Fig.13b-e), and this failure might be caused by relatively high inert stress and inadequate adhesive strength between CrBCN coatings and substrates [23]. Thus, although the incorporated boron could still contribute to lowering the friction coefficient of Cr-B-C-N/SiC tribopairs at higher loads (Fig.9), the wear resistance of CrBCN coatings was poor.

3.4 Discussion

As is known, the tribological performances of coatings were strongly determined by the coating composition, bonding structures and the formation of tribo-layers. By increasing the CrB_2 target current from 0 A to 4 A, the boron concentration of Cr-B-C-N coatings increased monotonically from 0 to 27.2%, while the concentrations of Cr, C and N elements all decreased sharply when the CrB_2 target current increased to 1 A, and then fluctuated slightly with further increasing CrB_2 target. Based on the analyses of XRD and XPS in Figs.1 and 2, the incorporated B mainly existed as amorphous B-N, B-O and B-C bonds. When the CrCN coating slid against SiC ball at the normal load of 3 N in tap water, the initial contact pressure was in the range of 0.66-0.70 GPa, and the tribochemical reactions between tribomaterials and water could occur easily and then there were a few grooves on the wear track of CrCN coating (Fig.11). When the CrB_2 target current increased to 1-4 A, fewer grooves could be observed on the worn surfaces of coatings. As seen in Fig.14a, the logarithmic value of specific wear rate increased linearly with

the friction coefficient, which was expressed as:

$$\ln(w_{s,d}) = -18.3 + 17.9\mu_m \quad (5)$$

This indicated that the abrasive wear was a main wear mechanism for Cr-B-C-N coatings. However, when the CrB_2 target current was beyond 1 A, the wear tracks on Cr-B-C-N coatings became smooth and flat in Fig.11(b-e). Thus, besides abrasive wear, the dominated wear mechanism for the Cr-B-C-N coatings also included tribochemical wear, and the transfer layer (Cr_2O_3, hydrated $Si(OH)_4$ and $B(OH)_3$) was formed at the sliding interface. The tribochemical reactions of CrCN coating and CrBCN coatings with water occurred as follows [26, 40]:

$$SiC + H_2O \rightarrow Si(OH)_4 + CH_4 \quad (6)$$

$$Cr_xCN_y + H_2O \rightarrow Cr_2O_3 + NH_3 + CH_4 \quad (7)$$

$$Cr_xBC_yN_z + H_2O \rightarrow (NH_4)H_2BO_3 + Cr_2O_3 + CO_2 \quad (8)$$

It is clear that $Si(OH)_4$ gels and H_3BO_3 formed on the wear surface acting as a lubricating layer, while Cr_2O_3 particles played a role of polishing. Moreover, a small amount of Ca^{2+} and Mg^{2+} in tap water could form lubricating $CaCO_3$ and $Mg(OH)_2$ on the sliding interface [50, 51]. As seen in Fig.8, with increasing CrB_2 target current to 3 A, the friction coefficients and the specific wear rates of Cr-B-C-N/SiC tribopairs decreased from 0.21 and 5.7×10^{-7} mm^3/Nm to 0.16 and 2.1×10^{-7} mm^3/Nm，respectively. This phenomenon might be attributed to the lubrication effect of reaction product of borides and water. Sanchez et al. [52] indicated that there was a lubricant layer at contact area which was assumed to boron acid (H_3BO_3). Since the lubricating effect of boron acid (H_3BO_3) film with layered-crystal structure on the sliding surface, the lubrication condition was improved effectively, and then the friction coefficient and wear rate of Cr-B-C-N/SiC tribopairs decreased [53-57]. In principle, the specific wear rate of coatings is closely related to their mechanical properties. According to Archard's equation [58], the specific wear rates of coatings

were influenced by their hardness. As seen in Fig.14b, the Logarithmic values of specific wear rate and 1/H displayed a linear relationship as:

$$\ln(w_{s,d}) = 114 + 5.5\ln(\frac{1}{H}) \quad (9)$$

It is obvious that the specific wear rates of coatings decreased rapidly with the increase of hardness. As a result, the specific wear rates of Cr-B-C-N/SiC tribopairs were lower when the current of CrB_2 target varied in the range of 2-3 A, because the hardness of CrBCN-2 and CrBCN-3 coatings was relatively higher compared to the rest coatings. In particular, CrBCN-3 showed the best wear resistance due to its lower friction coefficient and better mechanical properties. Furthermore, CrBCN-3 coating exhibited the maximum values of H/E and H^3/E^2, which contributed to its strong wear resistance as well. However, when the Cr-B-C-N coatings slid against SiC ball at 6 N, the initial contact pressure varied in the range of 0.83 to 0.88 GPa, and the wear resistance was poor (Fig.13) due to relatively lower load-bearing capacity in water environment [59]. Thus, although incorporated B still played a role in lowering friction coefficient at higher loads, the wear resistance of CrBCN coatings was poor due to inadequate adhesive strength to substrates, and the delamination became the main wear mechanism.

4. **Conclusions**

The Cr-B-C-N coatings with different boron contents were deposited on Si(100) wafers and 316L stainless steels using unbalanced magnetron sputtering system by way of adjusting the CrB_2 target currents, and their microstructure, mechanical and tribological properties of Cr-B-C-N coatings in water have been investigated, and the results are summarized as follows:

(1) With increasing the CrB_2 target current to 4 A, the boron content of Cr-B-C-N coatings increased from 0 at.% to 27.2 at.%, and the incorporated boron mainly existed as soft a-BN phases.

(2) When the CrB_2 target current varied in the range of 0-3 A, the hardness of Cr-B-C-N coatings fluctuated around 18 GPa, but the CrBCN-3 coatings' elastic modulus decreased to 231±4.89 GPa. With further increasing the CrB_2 target current to 4 A, the hardness and elastic modulus of coatings both decreased slightly.

(3) When the normal load was 3 N, the lowest friction coefficient of 0.16 and the lowest of specific wear rate of 2.1×10^{-7} mm^3/Nm were obtained simultaneously for the CrBCN-3/SiC tribopairs. The wear mechanism of Cr-B-C-N coatings was mainly tribochemical wear and abrasive wear.

(4) When the normal load increased to 6 N, the wear resistance of Cr-B-C-N coatings was poor due to the serious delaminations of coatings.

Acknowledgements

This work was supported by National Natural Science Foundation of China (Grant No. 51375231), The Research Fund for the Doctoral Program of Higher Education (Grant No.20133218110030). A Project Funded by Priority Academic Program Development of Jiangsu Higher Education Institutions (PAPD). We would like to acknowledge them for their financial support.

References

[1] D. Martínez-Martínez, L. Kolodziejczyk, J.C. Sánchez-López, A. Fernández, Tribological carbon-based coatings: An AFM and LFM study, Surf. Sci. 603 (7) (2009) 973-979.

[2] Q.Z. Wang, F. Zhou, C.D. Wang, M.F. Yuen, M.L. Wang, T. Qian, M. Matsumoto, J.W. Yan, Comparison of tribological and electrochemical properties of TiN, CrN, TiAlN and a-C:H coatings in simulated body fluid, Mater. Chem. Phys. 158 (5) (2015) 74-81.

[3] R. Hauert, A review of modified DLC coatings for biological applications, Mater. Chem. Phys.

12 (3-7) (2003) 583-589.

[4] W. Dai, P.L Ke, A.Y. Wang, Microstructure and property evolution of Cr-DLC films with different Cr content deposited by a hybrid beam technique, Vacuum 85 (8) (2011) 792-797.

[5] F. Zhou, K. Adachi, K. Kato, Sliding friction and wear property of a-C and a-CNx coatings against SiC balls in water, Thin Solid Films 514 (1-2) (2006) 231-239.

[6] Y.J. Wang, H.X. Li, X.H. Liu, L. Ji, Y.X. Wu, Y.H. Lv, Y.Y. Fu, H.D. Zhou, J.M. Chen, Friction and wear Properties of graphite-Like carbon films deposited on different substrates with a different interlayer under high Hertzian contact stress, Tribol. Lett. 46(3) (2012) 243-254.

[7] Y. Tanno, A. Azushim, Effect of counter materials on coefficients of friction of TiN coatings with preferred grain orientations, Wear 266(11-12) (2009) 1178–1184.

[8] S. Wilson, A.T. Alpas, Dry sliding wear of a PVD TiN coating against Si3N4 at elevated temperatures, Surf. Coat. Technol. 86-87 (1) (1996) 75-81.

[9] I. Dreiling, C. Raisch, J. Glaser, D. Stiens, T. Chassé, Characterization and oxidation behavior of MTCVD Ti–B–N coatings, Surf. Coat. Technol. 206 (2-3) (2011) 479–486.

[10] P.K.P. Rupa, P.C. Chakraborti, S.K. Mishra, Structure and indentation behavior of nanocomposite Ti–B–N films, Thin Solid Films 564 (2014) 160–169.

[11] I. Dreiling, C. Raisch, J. Glaser, D. Stiens, T. Chassé, Temperature dependent tribooxidation of Ti–B–N coatings studied by Raman spectroscopy, Wear 288 (2012) 62– 71.

[12] T. Polcar, T. Kubart, R. Novák, L. Kopecký, P. Široký, Comparison of tribological behaviour of TiN, TiCN and CrN at elevated temperatures, Surf. Coat. Technol. 193 (1-3) (2005) 192– 199.

[13] T. Polcar, R. Novák, P. Široký, The tribological characteristics of TiCN coating at elevated temperatures, Wear 260 (1-2) (2006) 40–49.

[14] L.F. Senn, C.A. Achetea, T. Hirsch, F.L. Freire, Structural, chemical, mechanical and

corrosion resistance characterization of TiCN coatings prepared by magnetron sputtering, Surf. Coat. Technol. 91-95 (1997) 390-397.

[15] K.H. Kim, J.T. Ok, S. Abraham, Y.R. Ch, I.W. Park, J.J. Moore, Syntheses and mechanical properties of Ti–B–C–N coatings by a plasma-enhanced chemical vapor deposition, Surf. Coat. Technol. 201(7) (2006) 4185–4189.

[16] J.L. Lin, J.J. Moore, B. Mishra, M. Pinkas, W.D. Sproul, Sproul, The structure and mechanical and tribological properties of TiBCN nanocomposite coatings, Acta Mater. 58 (5) (2010) 1554–1564.

[17] A. Vyas, Y.H. Lu, Y.G. Shen, Mechanical and tribological properties of multicomponent Ti–B–C–N thin films with varied C contents, Surf. Coat. Technol. 204 (9-10) (2010) 1528–1534.

[18] J.L. Lin, N.Y. Zhang, W.D. Sproul, J.J. Moore, A comparison of the oxidation behavior of CrN films deposited using continuous dc, pulsed dc and modulated pulsed power magnetron sputtering, Surf. Coat. Technol. 206 (14) (2012) 3283–3290.

[19] J.L. Lin, W.D. Sproul, J.J. Moore, Tribological behavior of thick CrN coatings deposited by modulated pulsed power magnetron sputtering, Surf. Coat. Technol. 206 (8-9) (2012) 2474–2483.

[20] Y.C. Chim, X.Z. Ding, X.T. Zeng, S. Zhang, Oxidation resistance of TiN, CrN, TiAlN and CrAlN coatings deposited by lateral rotating cathode arc, Thin Solid Films 517 (17) (2009) 4845–4849.

[21] Z.W Wu, F. Zhou, Q.Z Wang, Z.F. Zhou, J.W. Yan, L.K.Y Li, Influence of trimethylsilane flow on the microstructure, mechanical and tribological properties of CrSiCN coatings in water lubrication, Appl. Surf. Sci. 355 (2015) 516–530.

[22] F. Zhou, K.M. Chen, M.L. Wang, X.J. Xu, H. Meng, M. Yu, Z.D. Dai, Friction and wear properties of CrN coatings sliding against Si3N4 balls in water and air, Wear 265 (7-8) (2008)

1029–1037.

[23] P.F. Hu, B.L. Jiang, Study on tribological property of CrCN coating based on magnetron sputtering plating technique, Vacuum 85 (11) (2011) 994-998.

[24] J.W. Lee, C.H. Cheng, H.W. Chen, Y.C. Chand, J.G. Duhd, L.W. Ho, Effects of boron and nitrogen contents on the microstructures and mechanical properties of Cr-B-N nanocomposite thin films, Pro. Eng. 36 (2012) 360-367.

[25] Y.W. Ye, Y.X. Wang, H. Chen, J.L. Li, Y.R. Yao, C.T. Wang, Doping carbon to improve the tribological performance of CrN coatings in seawater, Tribol. Int. 90 (2015) 362-371.

[26] Q.Z. Wang, F. Zhou, X.D. Ding, Z.F. Zhou, C.D. Wang, W.J. Zhang, L.K.Y. Li, S.T. Lee, Microstructure and water-lubricated friction and wear properties of CrN(C) coatings with different carbon contents, Appl. Surf. Sci. 268 (2013) 579-587.

[27] C.H. Cheng, J.W. Lee, L.W. Ho, H.W. Chen, Y.C Chan, J.G. Duh, Microstructure and mechanical property evaluation of pulsed DC magnetronsputtered Cr–B and Cr–B–N films, Surf. Coat. Technol. 206 (7) (2011) 1711–1719.

[28] G.A. Zhang, L.P. Wang, P.X. Yan, Q.J. Xue, Structure and mechanical properties of Cr–B–N films deposited by reactive magnetron sputtering, J. Alloys Comp. 486 (1-2) (2009) 227–232.

[29] C. Higdon, B. Cook, J. Harringa, A. Russell, J. Goldsmith, J. Qu, P. Blau, Friction and wear mechanisms in $AlMgB_{14}$-TiB_2 nanocoatings, Wear 271 (9) (2011) 2111–2115.

[30] Z. Sheng, S.Q. Xie, C.Y. Pan, Probability theory and mathematical statistics, fourth ed, Higher Education Press, Beijing, 2008.

[31] J.W. Lee, C.H. Cheng, H.W. Chen, L.W. Ho, J.G. Duh, Y.C. Chan, The influence of boron contents on the microstructure and mechanical properties of Cr-B-N thin films, Vacuum 87 (2013) 191-194.

[32] J.L. Lin, W.D. Sproul, J.J. Moore, S. Lee, S. Myers, High rate deposition of thick CrN and Cr_2N coatings using modulated pulse power (MPP) magnetron sputtering, Surf. Coat. Technol. 205 (10) (2011) 3226-3234.

[33] Y. Birol, Sliding wear of CrN, AlCrN and AlTiN coated AISI H13 hot work tool steels in aluminium extrusion, Tribol. Int. 57 (2013) 101-106.

[34] H,C. Barshilia, N. Selvakumar, B. Deepthi, K.S. Rajam, A comparative study of reactive direct current magnetron sputtered CrAlN and CrN coatings, Surf. Coat. Technol. 201 (16) (2006) 2193-2201.

[35] X.R. Deng, H. Kousaka, T. Tokoroyama, N. Umehara, Deposition and tribological behaviors of ternary BCN coatings at elevated temperatures, Surf. Coat. Technol. 259 (PA) (2014) 2–6.

[36] Q. Yang, C.B. Wang, S. Zhang, D.M. Zhang, Q. Shen, L.M. Zhang, Effect of nitrogen pressure on structure and optical properties of pulsed laser deposited BCN thin films, Surf. Coat. Technol. 204 (11) (2010) 1863–1867.

[37] P.C. Tsai, W.J. Chen, J.H. Chen, C.L. Chang, Deposition and characterization of TiBCN films by cathodic arc plasma evaporation, Thin Solid Films 517 (17) (2009) 5044–5049.

[38] K.P. Budna, J. Neidhardt, P.H. Mayrhofer, C. Mitterer, Synthesis–structure–property relations for Cr–B–N coatings sputter deposited reactively from a Cr–B target with 20 at% B, Vacuum 82 (8) (2008) 771–776.

[39] Z.W. Wu, F. Zhou, K.M. Chen, Q.Z. Wang, Z.F. Zhou, J.W. Yan, L.K.Y. Li, Friction and wear properties of CrSiCN coatings with low carbon content as sliding against SiC and steel balls in water, Tribol. Int. 94 (2016) 176–186.

[40] F. Zhou, K. Adachi, K. Kato, Friction and wear behavior of BCN coatings sliding against ceramic and steel balls in various environments, Wear 261 (2006) 301–310.

[41] Y.M. Chen, Z.X. Zen, S.R. Yang, J.Y. Zhang, The tribological performance of BCN films under ionic liquids lubrication, Diamond Relat. Mater. 18 (1) (2009) 20–26.

[42] J.L. Xiao, C.B. Wang, Q. Shen, L.M. Zhang, Influence of nitrogen pressure on bonding structure and mechanical properties of pulsed laser deposited BCN thin films, Surf. Coat. Technol. 276 (2015) 141–144.

[43] S. Nakao, T. Sonoda, K. Tsugawa, J. Choi, T. Kato, Effects of nitrogen gas ratio on composition and microstructure of BCN films prepared by RF magnetron sputtering, Vacuum 84 (5) (2010) 642–647.

[44] Y. Sakamaotoa, M. Nose, T. Mae, E. Honbo, M. Zhou, K. Nogi, Structure and properties of Cr–B, Cr–B–N and multilayer Cr–B/Cr–B–N thin films prepared by r.f.-sputtering, Surf. Coat. Technol. 174 –175 (2003) 444–449.

[45] X.Y. Chen, Z.H. Wang, S.L. Ma, V. Ji, Microstructure, mechanical and tribological properties of Ti–B–C–N films prepared by reactive magnetron sputtering, Diamond Relat. Mater. 19 (10) (2010) 1336–1340.

[46] M.A. Mannan, H. Noguchi, T. Kida, M. Nagano, N. Hirao, Y. Baba, Growth and characterization of stoichiometric BCN films on highly oriented pyrolytic graphite by radiofrequency plasma enhanced chemical vapor deposition, Thin Solid Films 518 (15) (2010) 4163–4169.

[47] J. Lin, B. Mishra, J.J Moore, M. Pinkas, W.D. Sproul, Structure and properties of Ti–B–C–N nanocomposite coatings synthesized using pulsed closed field unbalanced magnetron sputtering (P-CFUBMS), Surf. Coat. Technol. 203 (5-7) (2008) 588–593.

[48] L. Chekour, C. Nouveau, A. Chala, C. Labidi, N. Rouag, M.A. Djouadi, Growth mechanism for chromium nitride films deposited by magnetron and triode sputtering methods, Surf. Coat.

Technol. 200 (1-4) (2005) 241-244.

[49] A.M.A. El-Rahman, R.H. Wei, Effect of ion bombardment on structural, mechanical, erosion and corrosion properties of Ti-Si-C-N nanocomposite coatings, Surf. Coat. Technol. 258 (2014) 320-328.

[50] M. Uchidate, H. Liu, K. Yamamoto, A. Iwabuchi, Effects of hard water on tribological properties of DLC rubbed against stainless steel and brass, Wear 308 (1-2) (2013)79–85.

[51] M.A. Tofighy, T. Mohammadi, Permanent hard water softening using carbon nanotube sheets, Desalination. 268 (1-3) (2011) 208–213.

[52] J.L. He, S. Miyake, Y. Setsuhara, I Shimizu, M Suzuki, K Numata, H Saito, Improved anti-wear performance of nanostructured titanium boron nitride coatings, Wear 249 (5-6) (2001) 498–502.

[53] C.M.T. Sanchez, H.D.F. Filho, M.E.H.M.D. Costa, F.L.F Jr, Nitrogen incorporation into titanium diboride films deposited by dc magnetron sputtering: Structural modifications, Thin Solid Films 517 (19) (2009) 5683–5688.

[54] D.C. Reigada, R. Prioli, L.G. Jacobsohn, F.L. Freire Jr, Boron carbide films deposited by a magnetron sputter–ion plating process: film composition and tribological properties, Diamond Relat. Mater. 9 (3-6) (2000) 489–493.

[55] A. Erdemir, C. Bindal, G. R. Fenske, Formation of ultralow friction surface films on boron carbide, Appl. Phys. Lett. 68 (12) (1996) 1637-1639.

[56] X.D. Ma, W.N. Unertl, The boron oxide–boric acid system: Nanoscale mechanical and wear properties, J. Mater. Res. 14 (8) (1999) 3455-3466.

[57] Q. Ma, F. Zhou, S. Gao, Z.W. Wu, Q.Z. Wang, K.M. Chen, Z.F. Zhou, L.K.Y. Li, Influence of boron content on the microstructure and tribological properties of Cr-B-N coatings in water

lubrication, Appl. Surf. Sci. 377 (2016) 394-405.

[58] J. F. Archard, Contact and Rubbing of Flat Surfaces, J. Appl. Phys. 24 (8) (1953) 981-988.

[59] Y.X. Wang, J.B. Pu, J.F. Wang, J.L. Li, J.M. Chen, Q.J. Xue, Interlayer design for the graphite-like carbon film with high load-bearing capacity under sliding-friction condition in water, Appl. Surf. Sci. 311 (2014) 816-824.

Table 1 Deposition parameters of Cr-B-C-N coatings

Parameter	Figure
Chamber pressure	0.17 Pa
Temperature	150 □
Bias voltage	−80 V
Rotating speed of holder	10 rpm
Optical emission monitor (OEM)	50%
Current of Cr target	4A
Current of C target	4A
Current of CrB_2 target	0-4A

Table 2 Thickness and element concentration of Cr-B-C-N coatings deposited at different CrB_2 target currents

Coatings	Thickness (μm)	B (at.%)	C (at.%)	N (at.%)	Cr (at.%)
CrCN	1.40	0	29.8	26.5	43.7
CrBCN1	1.50	24.6	20.4	20.6	34.4
CrBCN2	1.50	24.9	22.0	19.8	33.3
CrBCN3	1.59	25.1	20.9	19.1	34.9
CrBCN4	1.61	27.2	22.7	18.0	32.1

Table 3 Hardness, elastic modulus, H/E and H^3/E^2 of Cr-B-C-N coatings deposited at different CrB_2 target currents

coatings	Hardness, H(GPa)	Elastic modulus, E (GPa)	H/E	H^3/E^2 (GPa)
CrCN	17.7±1.03	258±9.59	0.068	0.083
CrBCN1	17.9±0.79	256±7.37	0.070	0.088
CrBCN2	18.6±0.86	261±10.40	0.071	0.094
CrBCN3	18.2±0.56	231±4.89	0.079	0.113
CrBCN4	16.3±0.28	228±2.53	0.071	0.083

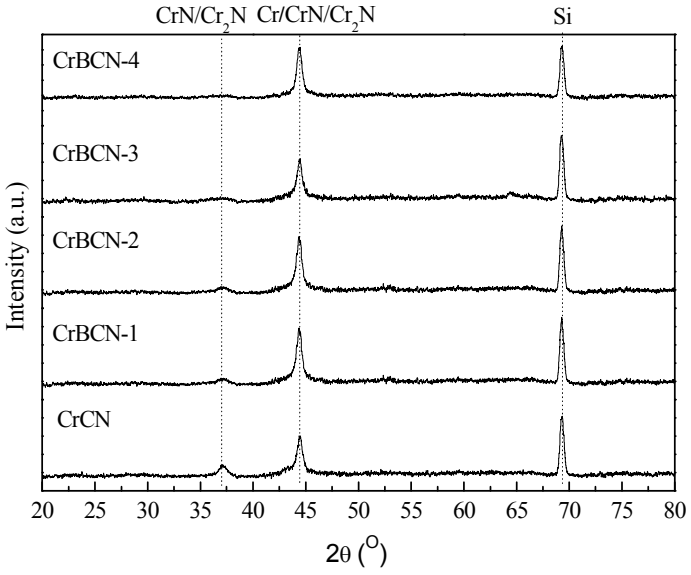

Fig.1. X-ray diffraction spectra of Cr-B-C-N coatings deposited at different CrB_2 currents.

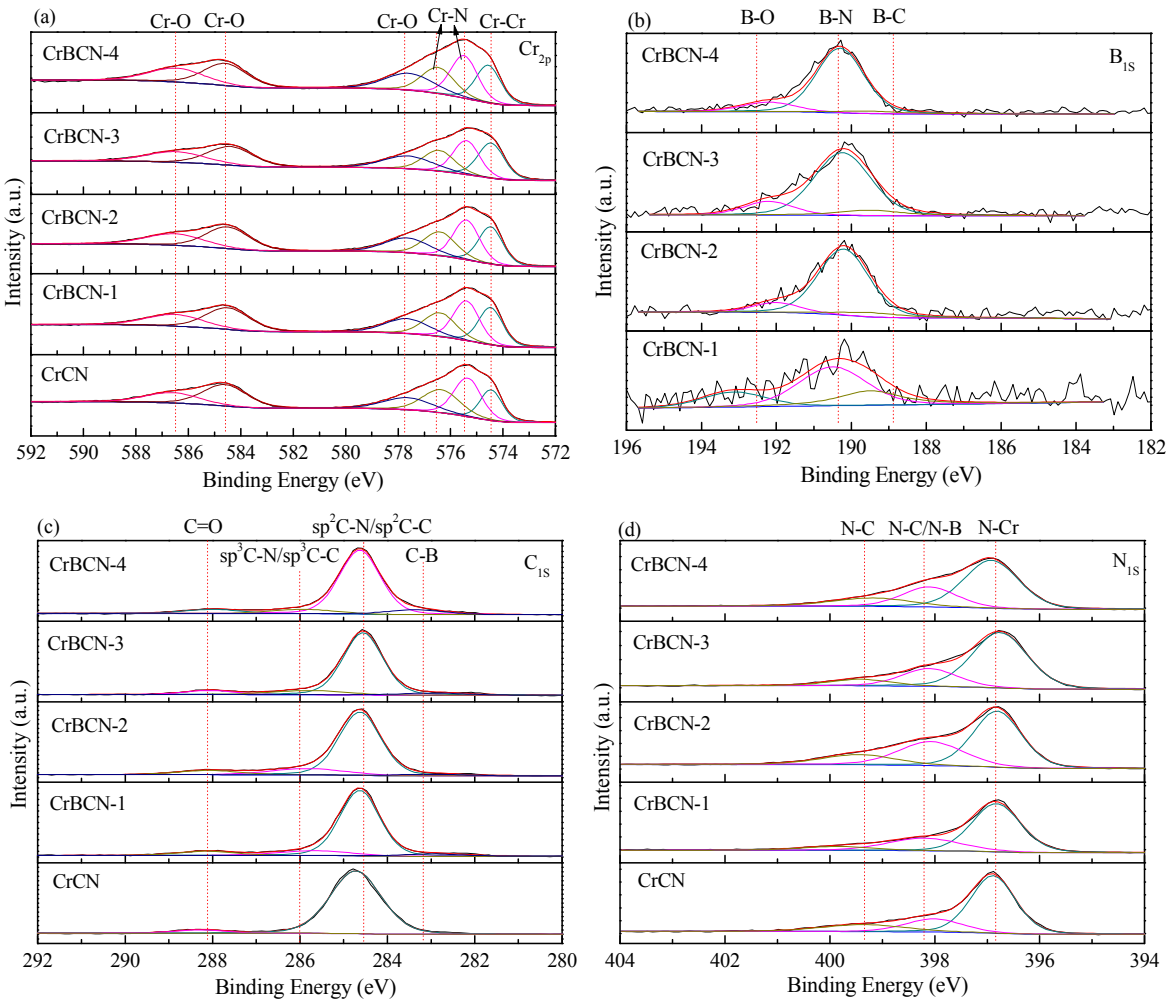

Fig.2. XPS spectra of Cr-B-C-N coatings deposited at different CrB_2 target currents.

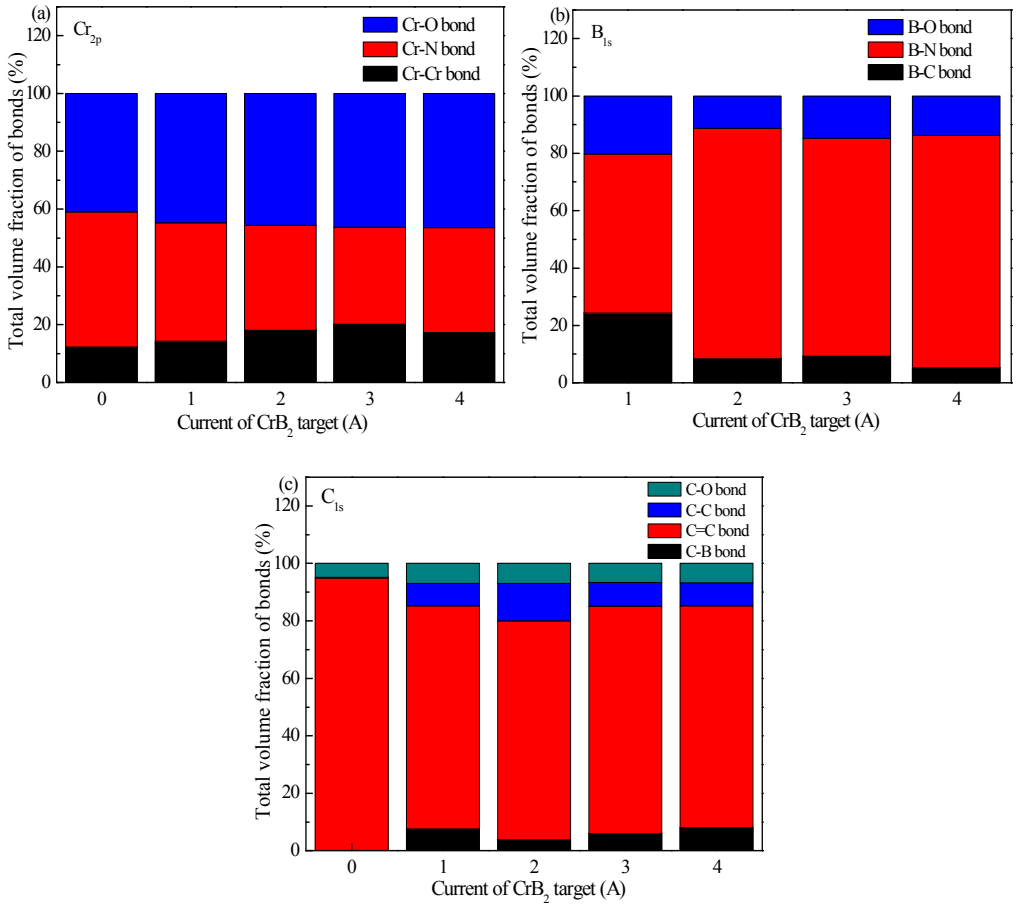

Fig.3. XPS analysis results of B_{1s} (a), N_{1s} (b) and C_{1s} (c) of Cr-B-C-N coatings at different CrB_2 target currents.

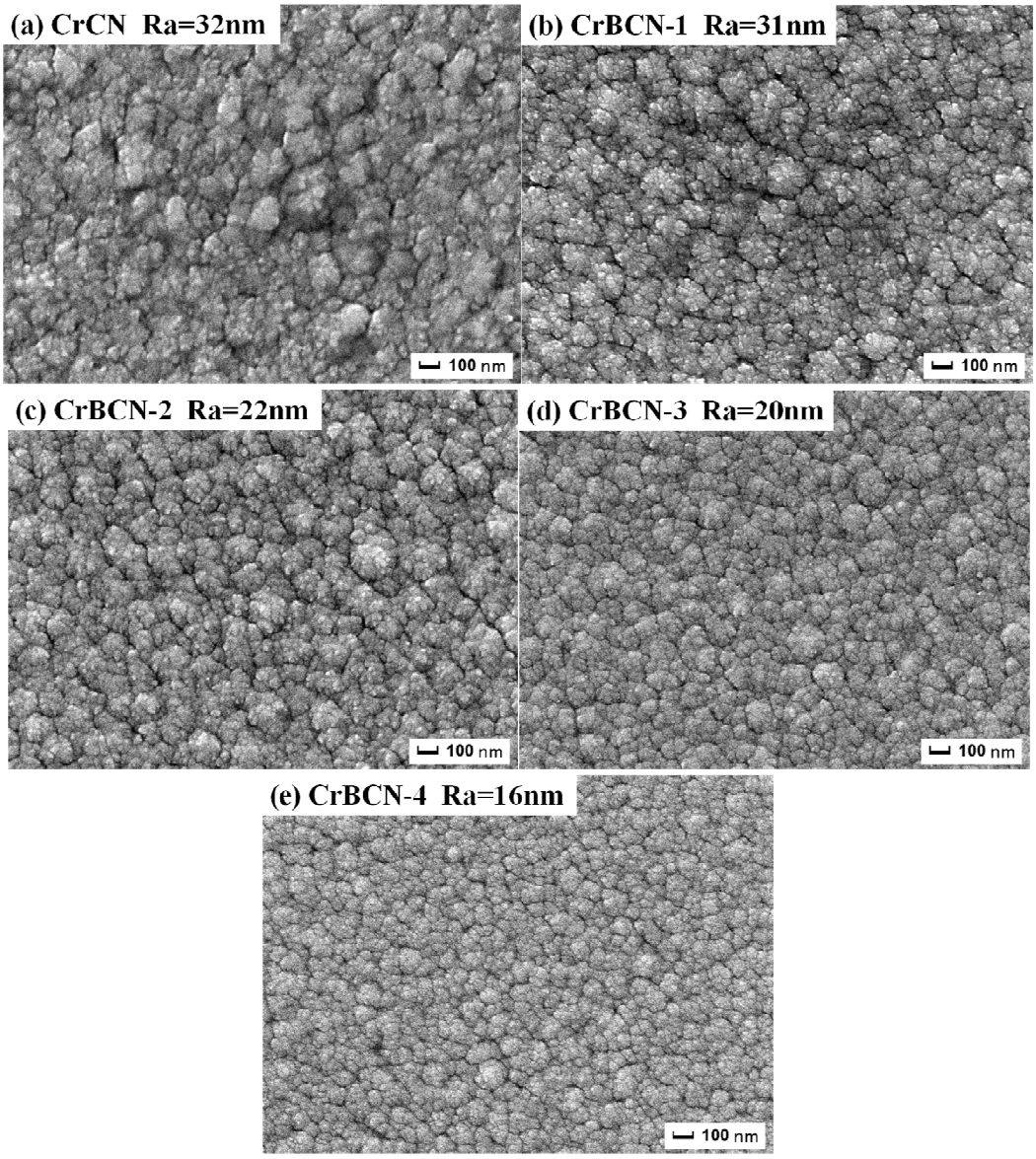

Fig.4. SEM images of topography and the corresponding surface roughness of Cr-B-C-N coatings.

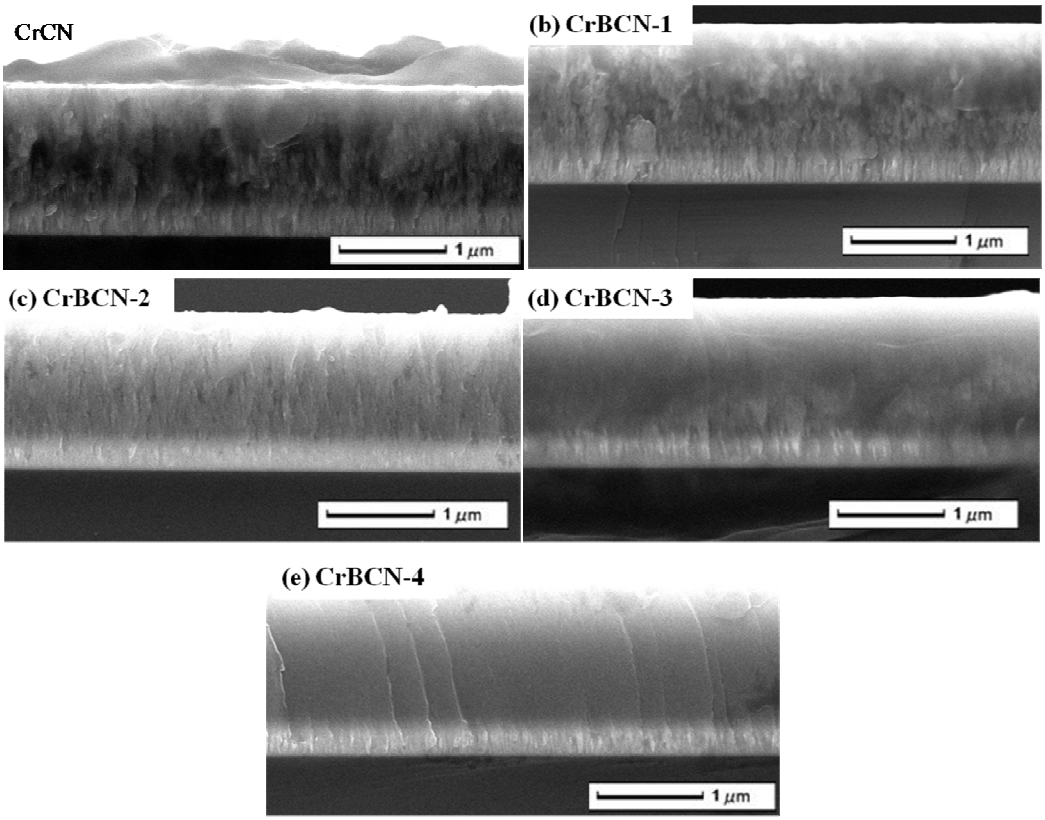

Fig.5. Cross-sectional microstructure of Cr-B-C-N coatings deposited at different CrB_2 target currents.

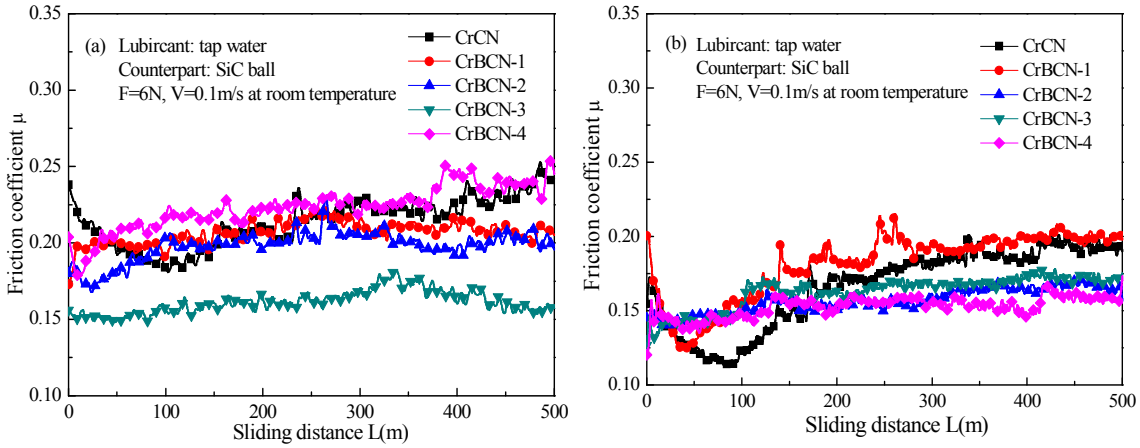

Fig.6. Influence of CrB_2 target currents on the friction behavior of Cr-B-C-N/SiC tribopairs at the normal load of 3N (a) and 6N (b) in tap water.

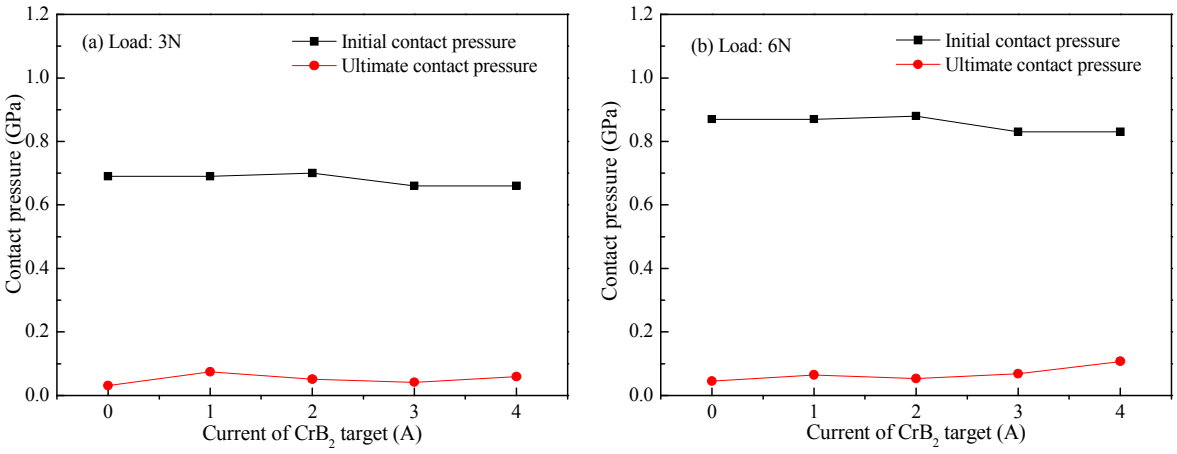

Fig.7. Contact pressure of the Cr-B-C-N/SiC tribopairs at 3N (a) and 6N (b) in tap water.

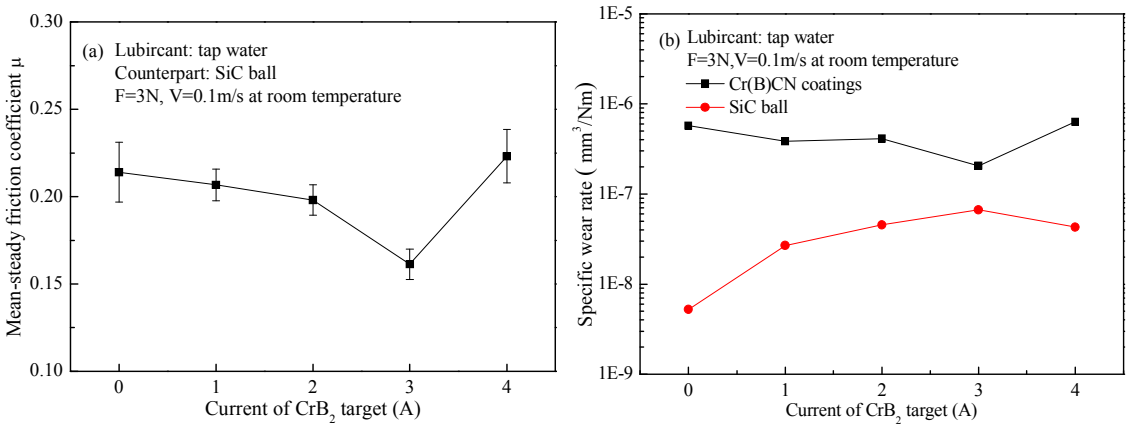

Fig.8. Influence of CrB_2 target currents on mean-steady friction coefficient (a) and specific wear rate (b) of Cr-B-C-N/SiC tribopairs at the normal load of 3N in tap water.

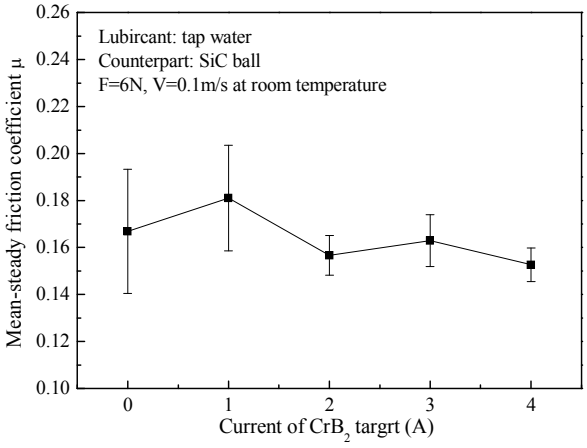

Fig.9. Influence of CrB_2 target currents on mean-steady friction coefficient of Cr-B-C-N/SiC tribopairs at the normal load of 6N in tap water.

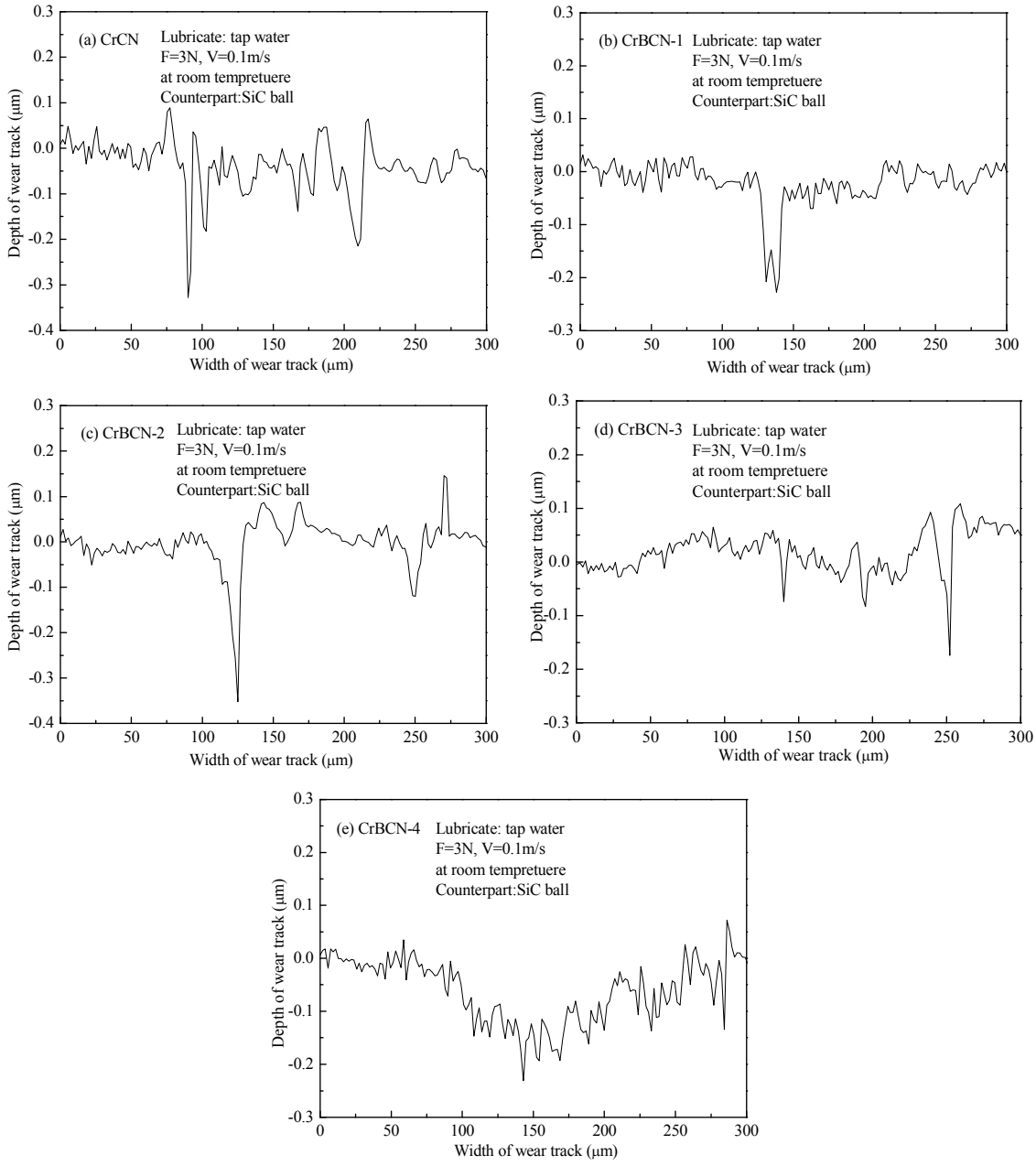

Fig.10. Influence of CrB_2 target currents on the cross sectional profiles of wear track on Cr-B-C-N coatings sliding against SiC balls at 3N in tap water.

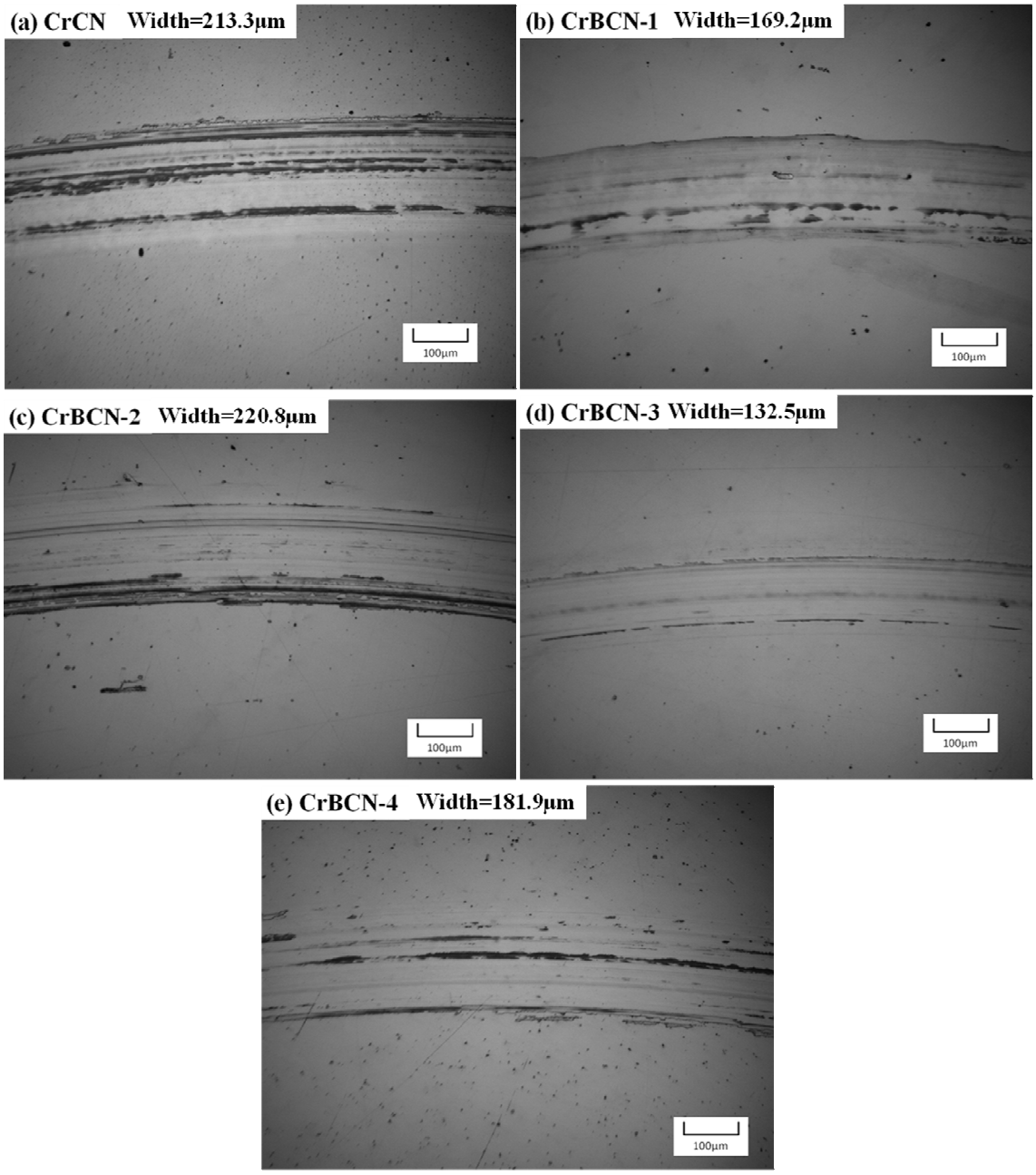

Fig.11. Optical images of wear track for Cr-B-C-N coatings sliding against SiC balls at the normal load of 3N in tap water.

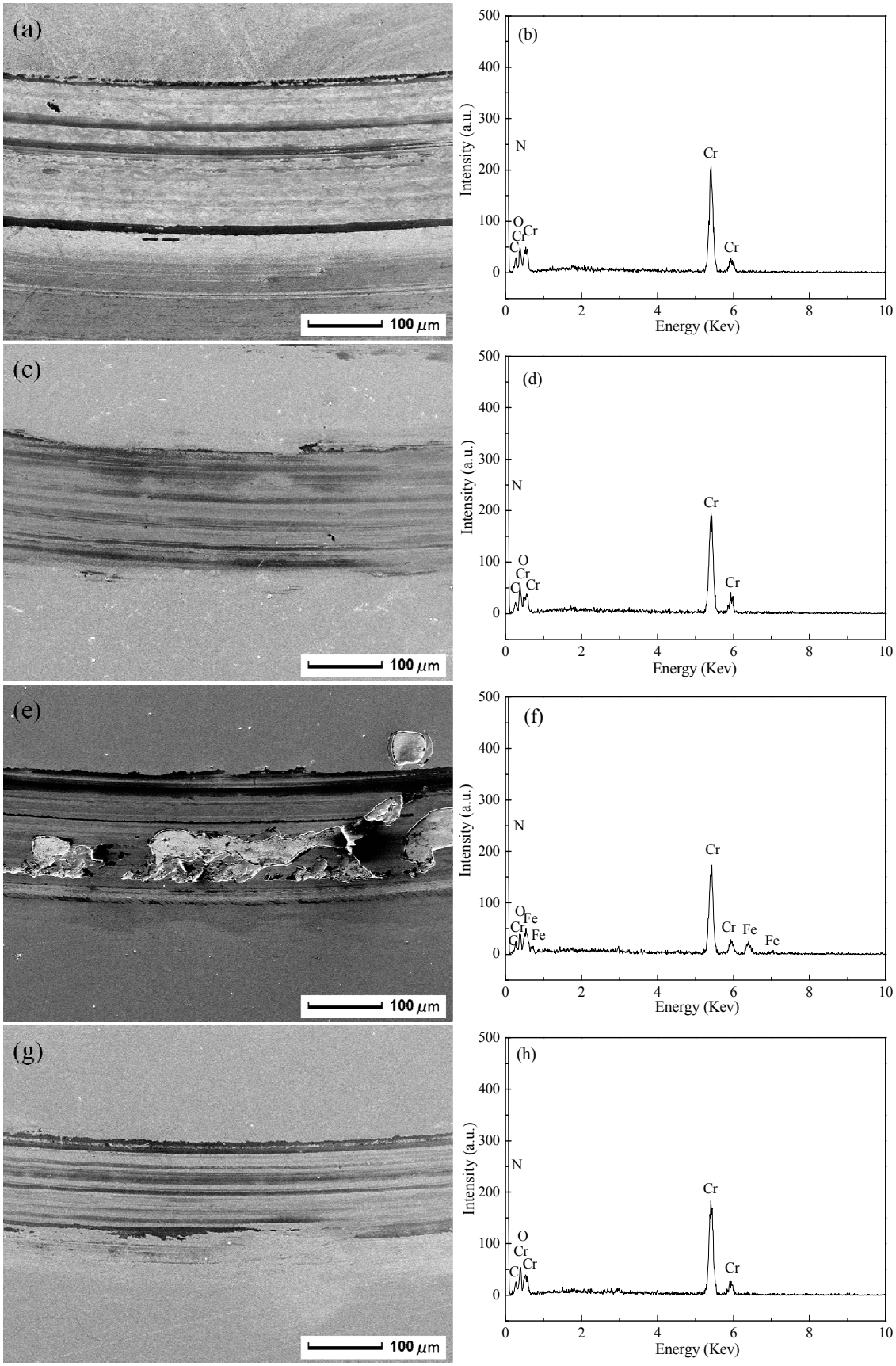

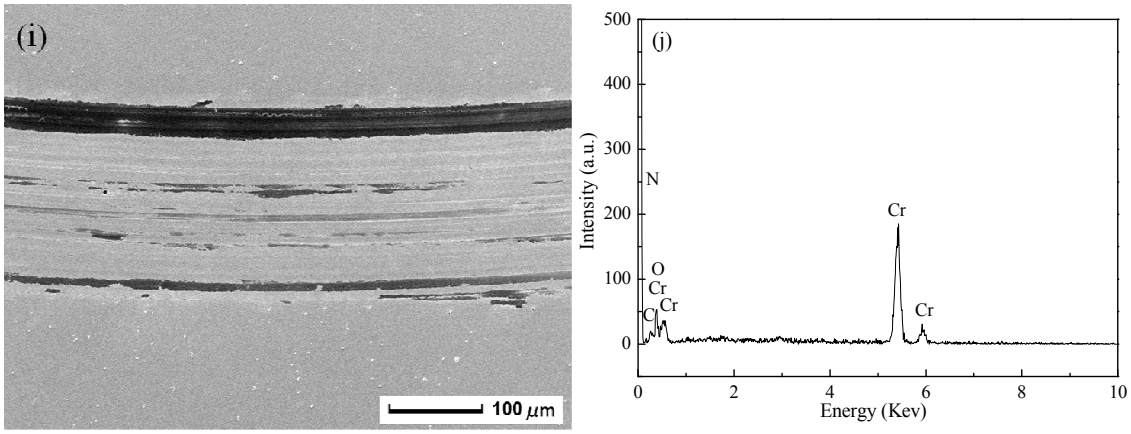

Fig.12. SEM images and corresponding EDS analysis of wear track for CrCN(a) (b), CrBCN-1(c) (d), CrBCN-2(e) (f), CrBCN-3(g) (h), CrBCN-4 (i) (j) coatings sliding against SiC balls at the normal load of 3N.

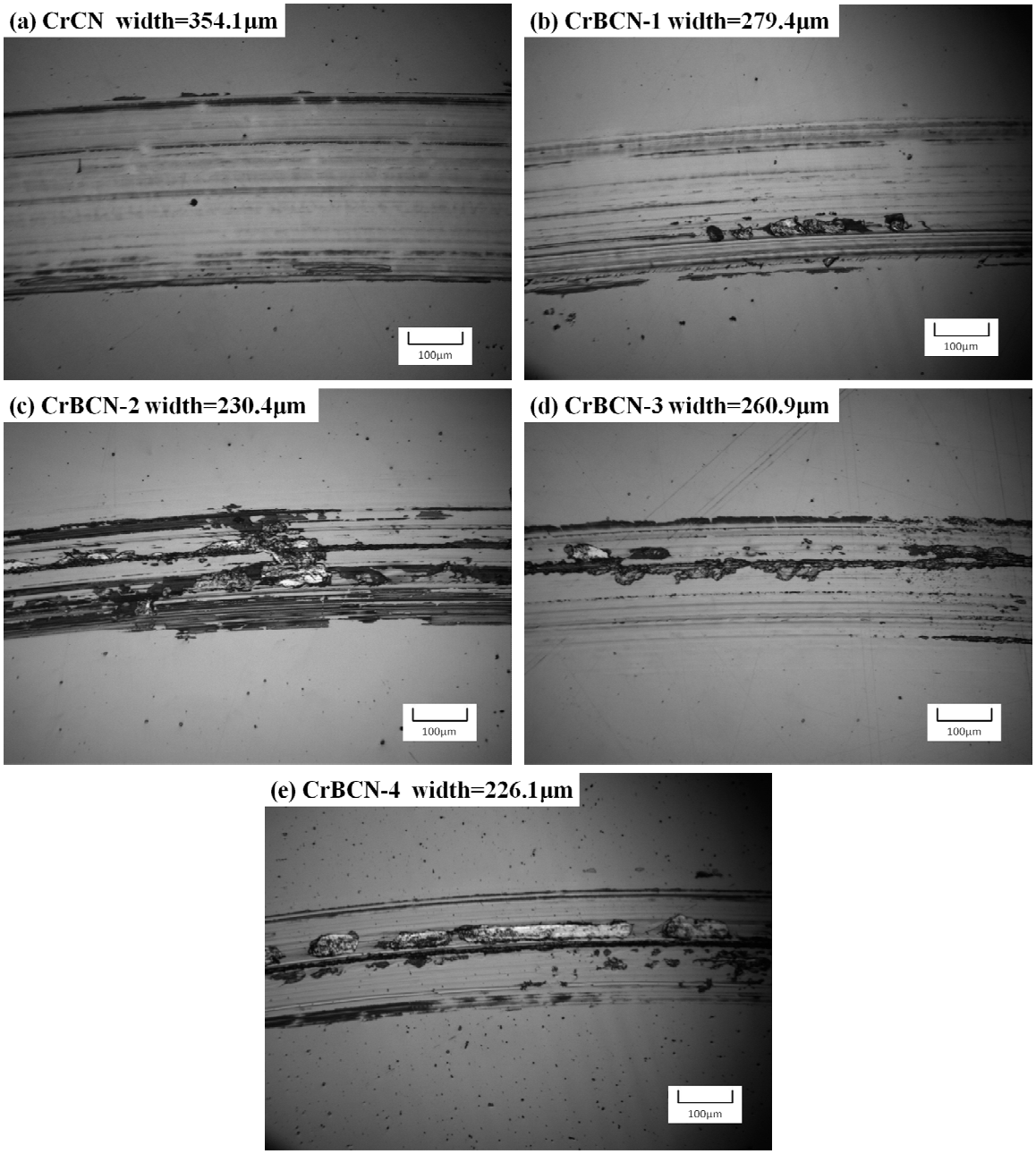

Fig.13. Optical images of wear track for Cr-B-C-N coatings sliding against SiC balls at the normal load of 6N in tap water.

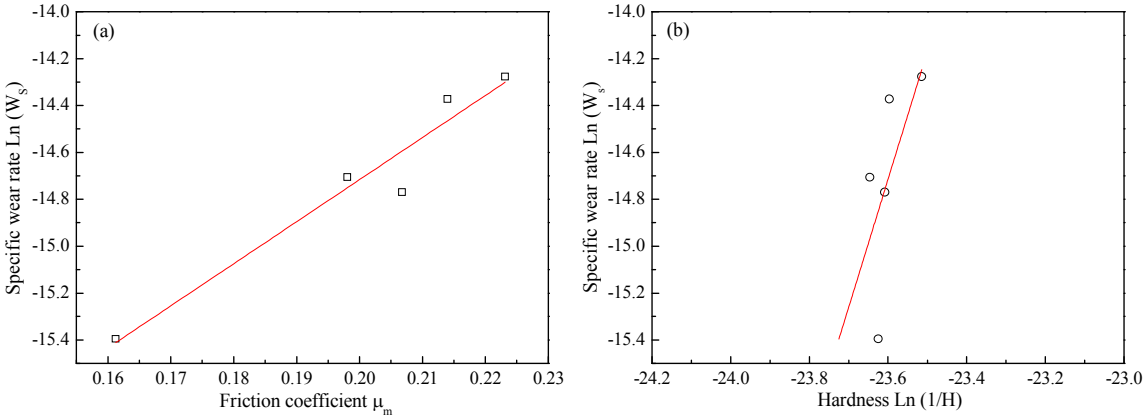

Fig.14. (a) Logarithmic relationship of specific wear rate against friction coefficient (μm), (b) Logarithmic relationship between specific wear rate and 1/H (H is the hardness of coatings).